Numerical Simulation of Air–Sea Coupling during Coastal Upwelling

NATALIE PERLIN AND ERIC D. SKYLLINGSTAD

College of Oceanic and Atmospheric Sciences, Oregon State University, Corvallis, Oregon

ROGER M. SAMELSON

College of Oceanic and Atmospheric Sciences, and Cooperative Institute for Oceanographic Satellite Studies, Oregon State University, Corvallis, Oregon

PHILIP L. BARBOUR

Wind Research Cooperative, Oregon State University, Corvallis, Oregon

(Manuscript received 31 May 2006, in final form 25 September 2006)

ABSTRACT

Air–sea coupling during coastal upwelling was examined through idealized three-dimensional numerical simulations with a coupled atmosphere–ocean mesoscale model. Geometry, topography, and initial and boundary conditions were chosen to be representative of summertime coastal conditions off the Oregon coast. Over the 72-h simulations, sea surface temperatures were reduced several degrees near the coast by a wind-driven upwelling of cold water that developed within 10–20 km off the coast. In this region, the interaction of the atmospheric boundary layer with the cold upwelled water resulted in the formation of an internal boundary layer below 100-m altitude in the inversion-capped boundary layer and a reduction of the wind stress in the coupled model to half the offshore value. Surface heat fluxes were also modified by the coupling. The simulated modification of the atmospheric boundary layer by ocean upwelling was consistent with recent moored and aircraft observations of the lower atmosphere off the Oregon coast during the upwelling season. For these 72-h simulations, comparisons of coupled and uncoupled model results showed that the coupling caused measurable differences in the upwelling circulation within 20 km off the coast. The coastal Ekman transport divergence was distributed over a wider offshore extent and a thinner ocean surface boundary layer, with consistently smaller offshore and depth-integrated alongshore transport formed in the upwelling region, in the coupled case relative to the uncoupled case. The results indicate that accurate models of coastal upwelling processes can require representations of ocean–atmosphere interactions on short temporal and horizontal scales.

1. Introduction

In a classical wind-driven upwelling system, sustained southward winds along the eastern ocean boundary lead to offshore transport in the surface ocean layer and result in upward transport of colder bottom waters near the coast. This coastal circulation and the associated meteorological forcing have been the subject of numerous observational, theoretical, and modeling studies (e.g., Smith 1974; Halpern 1976; Huyer 1983; Lentz 1995; Enriquez and Friehe 1995; Allen et al. 1995; Federiuk and Allen 1995; Gan et al. 2005). This research, motivated in part by the desire to understand the functioning of highly productive coastal upwelling ecosystems, has led to the discovery of an intricate chain of interdependent physical processes in both the coastal ocean and atmosphere.

Recent in situ and aircraft observations of surface air temperature (SAT), sea surface temperature (SST), and coastal marine atmospheric boundary layer properties have suggested a systematic response of the coastal atmosphere to the cold surface waters that develop from wind-driven upwelling along the Oregon coast (Samelson et al. 2002; Bane et al. 2005). On larger space and time scales, satellite observations indicate

Corresponding author address: Dr. Natalie Perlin, College of Oceanic and Atmospheric Sciences, Oregon State University, 104 COAS Admin. Bldg., Corvallis, OR 97331-5503.
E-mail: nperlin@coas.oregonstate.edu

DOI: 10.1175/JPO3104.1

that variations in SST can have a significant effect on the surface wind stress (Chelton et al. 2001, 2007). These observations suggest that cool water generated through upwelling could cause substantial variations in wind stress and thereby alter the fundamental aspects of the coastal circulation. Our primary goal in this paper is to understand the dynamics of this process and assess the importance of modeling the coupled circulation rather than the traditional approach of examining the ocean response to imposed atmospheric forcing.

Many factors affect the scale and evolution of upwelling circulations. We concentrate here on the interaction between the atmospheric marine boundary layer and the upper ocean in the upwelling region over spatial scales up to several tens of kilometers and time scales up to 3 days. Our main objective is to examine the development of temporally and spatially variable air–sea fluxes induced by the response of the coastal ocean to upwelling-favorable wind stress and to assess their short-term effect on the coastal circulation. We utilize a two-way coupled modeling system, implemented for idealized coastal simulations. The main focus is on the coupled response of the ocean–atmosphere system, without external effects, such as the role of bottom bathymetry changes or coastline features. We examine the basic physics of the coupled response and its characteristic spatial and temporal scales under idealized conditions representative of the U.S. West Coast.

The paper is organized as follows. Section 2 briefly describes the model components and coupling strategy. Section 3 elaborates on model settings and initial conditions for the presented simulations. Section 4 discusses model results, section 5 contains a discussion, and section 6 summarizes the findings of the study and further modeling plans.

2. System components and model coupling strategy

The coupled model system consists of atmospheric and ocean components interconnected through an interface program. For the atmospheric component, we used the Naval Research Laboratory (NRL) Coupled Ocean–Atmosphere Mesoscale Prediction System (COAMPS; Hodur 1997). The ocean model component is the Regional Ocean Modeling System (ROMS; Shchepetkin and McWilliams 2005). The interface program connecting these two subcomponents was implemented using the Model Coupling Toolkit (MCT; Larson et al. 2005; http://www-unix.mcs.anl.gov/mct).

COAMPS is a three-dimensional mesoscale atmospheric model that has been successfully applied in both idealized cases and real-data simulations, including the coastal ocean area that is of our interest (Burk et al. 1999; Samelson et al. 2002; Pickett and Paduan 2003). COAMPS is based on the nonhydrostatic, fully compressible equations and a variety of physical parameterizations of subgrid-scale processes. The vertical model grid utilizes a terrain-following (σ–z) vertical coordinate system, stretched from the ground upward; a staggered Arakawa C grid is used in the horizontal plane. Turbulence in the atmospheric model is parameterized using the 1.5-order closure 2.5-level scheme (Mellor and Yamada 1982), with surface fluxes calculated using a modified Louis (1979) scheme. Boundary layer height calculations are based on the Richardson number. Radiative transfer parameterizations for both longwave and shortwave radiation follow the methods of Harshvardhan et al. (1987). Fourth-order horizontal diffusion is used to control the removal of high-frequency modes. Other model features include nesting capabilities, explicit moist physics calculations, and convective parameterizations, although these were not used in idealized simulated conditions presented here.

ROMS is a hydrostatic, Boussinesq, free-surface primitive equation ocean model originally designed for use in coastal regions. ROMS divides the baroclinic momentum and tracer equations from the barotropic momentum and continuity equations, using a split-explicit time-stepping algorithm. A topography-following stretched coordinate system is used, with enhanced vertical resolution near the surface to focus on air–sea coupling processes. The model uses Arakawa C staggering of mass and momentum variables. The present experiments utilize third-order upstream bias advection scheme for momentum and scalars (temperature and salinity) and harmonic (Laplacian) horizontal mixing. Vertical turbulent mixing followed Mellor–Yamada 2.5 scheme. An option for using K-profile method (KPP; Large et al. 1994) was also exercised but was found to have difficulties representing the ocean surface boundary layer in the presence of diurnal variability of solar heating.

The MCT software used to couple the oceanic and atmospheric models is a set of FORTRAN90 modules developed as a flux coupler between different earth system models for use with parallel computing systems. MCT tasks include governing the overall execution and control of the coupled model, synchronization and communication of data between the components, time averaging and accumulation of data from one component for subsequent transmission to other components, computation of interfacial fluxes, and interpolation of flux and state data between various component model grids.

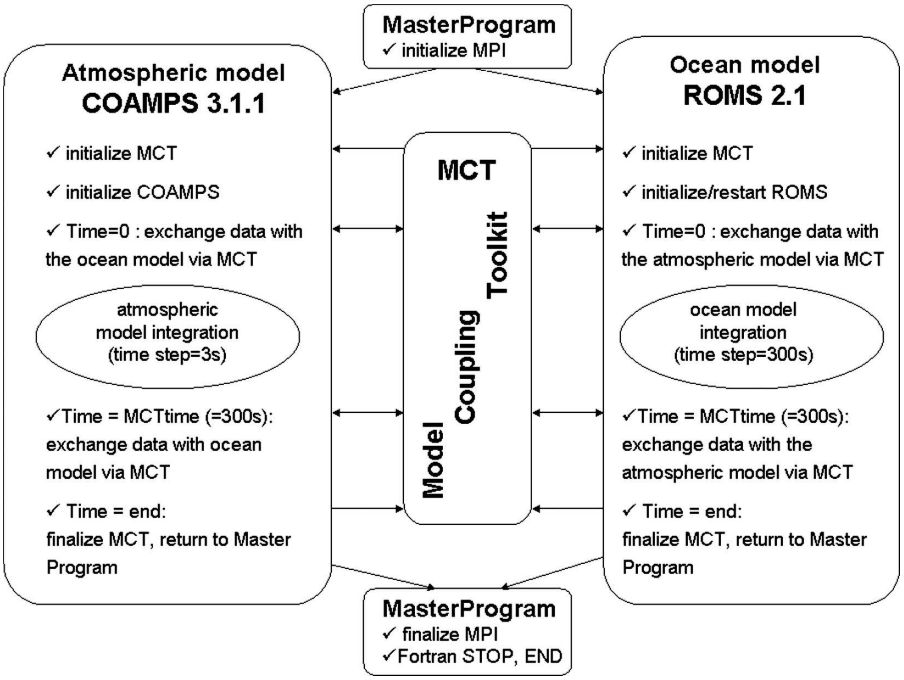

FIG. 1. A flowchart of the coupled code that forms a single-executable modeling system; its components run in concurrent mode.

The coupled model is a single-executable system designed to run in a concurrent mode with calculations of the atmospheric and ocean model components performed simultaneously on different processors (Fig. 1). The master program initializes the message passing interface (MPI), an operating system tool for parallel processing, and then transfers execution to the component models. Each of the models contacts the MCT to initialize model decomposition for the coupled system on a given number of processors, which can differ from the primary component model domain decomposition. Prescribed interpolation matrices for remapping fields between model grids are computed separately and stored in compact form for later use by MCT during data exchange sessions. In simulations having identical horizontal grids in both the ocean and atmosphere models, remapping is not necessary, but nonetheless has been performed here for test purposes using a simple unity matrix (all unit weights). As currently implemented, at least two processors are needed to run this system, one for each of the model components. Decomposition of the atmospheric domain into smaller subdomains can be performed for large model grids to utilize several processors and accelerate the calculations, but the present ocean model implementation is limited to single processor use. The ocean model integration usually takes notably less time than that of the atmospheric model, partially because of the longer ocean model time step, reducing the need to use more than a single processor for the ocean model.

Following the MCT and component model initializations, the ocean and atmosphere components are integrated forward for 300 s, which corresponds to 1 ocean model time step and 100 atmosphere model time steps. Data exchange and the corresponding remapping of fields are then performed, and model integration resumes for the next 300 s. This process is repeated until the final forecast time. During each data exchange, the atmospheric model supplies the ocean component with instantaneous forecast values of momentum flux, net longwave and net shortwave radiations, and sensible and latent heat fluxes, and the ocean model updates the SST field that is used for the surface boundary condition in the atmospheric model. At the completion of coupled model integration, MCT is finalized in both components, and subsequent control is returned to the master program that stops MPI and frees all computer memory reserved for the given numerical task.

3. Numerical experiment description and model setup

We consider a basic numerical experiment designed to simulate the development of wind-driven coastal upwelling circulation, formation of a well-mixed marine atmospheric boundary layer, and subsequent evolution

of the coupled system in response to the narrow region of cold water near the coast. In addition to the coupled simulation, in which surface momentum and heat fluxes from the atmospheric model were passed to the ocean and the updated ocean model SST was passed to the atmospheric model, an uncoupled simulation was performed for comparison. In the uncoupled case, all the air–sea fluxes were passed to the ocean, but the SST was held constant in the atmospheric model, not updated from the ocean model. In both cases, the air–sea fluxes were computed in the atmospheric model, using the continuously updated SST in the coupled case, and the constant SST in the uncoupled case.

The horizontal domain represented an idealized coastal ocean with no land, measuring 50 km × 20 km in cross-shore latitudinal (x) and alongshore longitudinal (y) directions, respectively, using 1-km by 1-km horizontal model grid boxes. The atmospheric model had 47 vertical σ layers extending to over 9000-m height, with 31 levels below 1 km. The ocean model had 40 vertical levels with an ocean bottom sloping linearly offshore, from 10-m depth at the coast to about 300-m depth 50 km offshore. This approximation of bathymetry was derived from real bathymetric database averaged in latitudinal direction between 43° and 46°N. Higher-level polynomials did not introduce significant changes to the linear fit. North–south lateral boundary conditions in both the ocean and atmosphere models were periodic, making the model domain a periodic channel in the alongshore direction. Model variables, forcing, and boundary conditions were all uniform alongshore, so that the simulations were numerically two-dimensional. The 20 along-channel grid points were included to assure proper numerical execution of the atmospheric model code. Radiation boundary conditions in the east–west direction were applied in the atmospheric model (Hodur 1997; Miller and Thorpe 1981). In the ocean model, a rigid coastal boundary was used in the east with open western boundary conditions consisting of zero gradients for the free surface and radiation conditions for momentum and tracers (Marchesiello et al. 2001).

The atmospheric model was initialized from a linear profile of temperature and a reconstructed profile of moisture, approximating typical coastal summertime conditions off the Oregon coast (Figs. 2a,b). A constant geostrophic pressure gradient was imposed corresponding to northerly winds of 15 m s^{-1}. To compensate for the average atmospheric radiative cooling in the absence of large-scale subsidence or advection, a uniform radiative heating term of 1°C day^{-1} was added everywhere. Although low-level stratus clouds are frequently observed over coastal waters, cloud formation physics

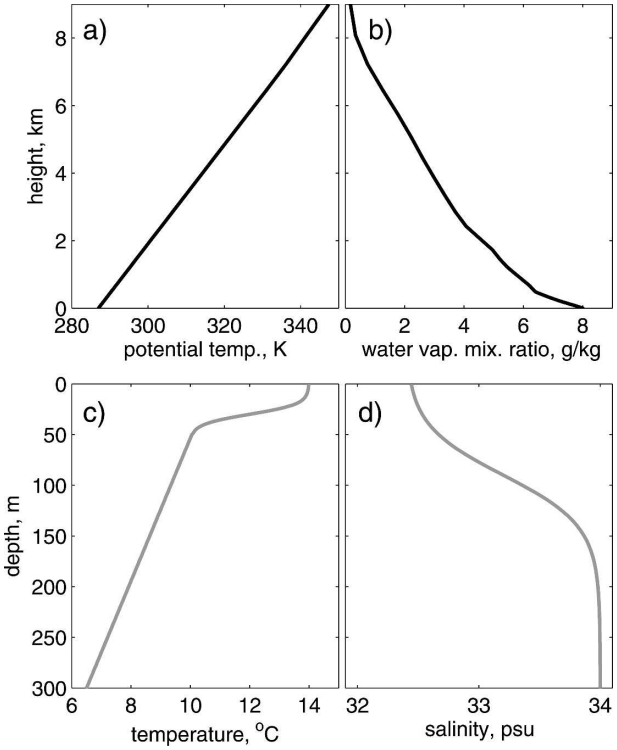

FIG. 2. Initial profiles used for horizontally homogeneous model initialization of (a) atmospheric potential temperature, (b) atmospheric water vapor mixing ratio, (c) ocean temperature, and (d) ocean salinity.

was disabled in the model. In our initial experiments, we found that the idealized, limited domain caused the formation of stratus clouds that complicated interpretation of air–sea interaction. Because the main emphasis of this paper is on boundary layer processes, we used an initial atmospheric moisture profile that was slightly drier than observations and also limited the moisture physics in COAMPS to prevent cloud formation and latent heating. Surface latent heat fluxes and water vapor were included, but cloud and rain formation were not permitted. In future work we plan to revisit this issue and investigate the effects that coupling has on cloud and fog formation.

Initialization of temperature and salinity in the ocean model was horizontally homogeneous, with profiles that approximately correspond to summertime conditions in the Oregon coastal zone (Figs. 2c,d). The temperature profile reflected a 20-m mixed layer, a moderately sharp thermocline between 20 and 50 m, and a weak linear temperature gradient below 50-m depth. The salinity profile had a deeper mixed layer, down to about 50 m, a halocline between 50 and 150 m, and nearly uniform salinity to the ocean bottom. Low salinity values near the surface reflected Columbia River

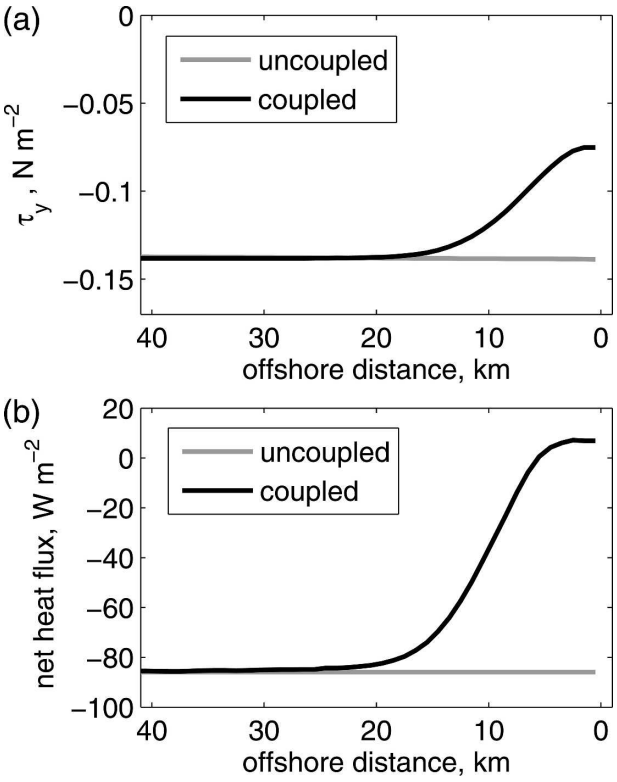

FIG. 3. Atmospheric surface forcing variables at the end of a 72-h run for two simulations: (a) surface meridional wind stress from the atmospheric model and (b) downward surface net heat flux (positive downward). Note that this model time corresponds to 0400 LST, and therefore solar radiation is zero at that time. Negative net heat fluxes into the ocean correspond to heat loss by the ocean and thus unstable conditions in general.

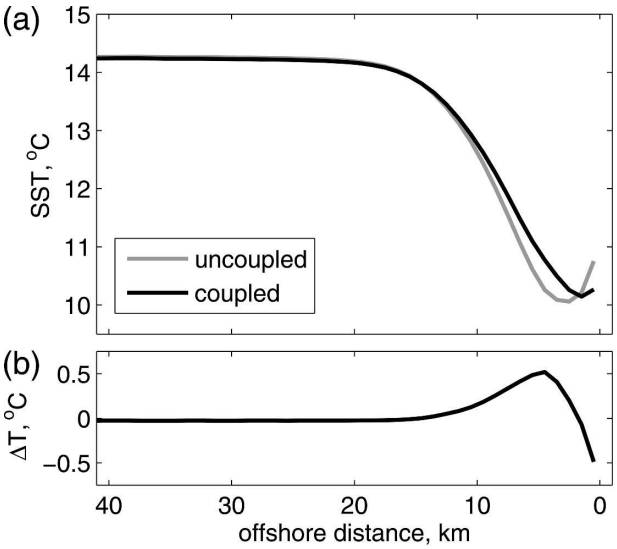

FIG. 4. (top) Cross-shore ocean model SST 72-h forecast for the simulations. (bottom) Temperature difference between the cases in the top panel.

outflow. The ocean was assumed to be at rest at the beginning of simulations. Because of the small longitudinal extent of the domain, the Coriolis parameter was taken to be constant in the ocean model. Simulations started at 0400 LST and terminated after 72 h. Model output was archived every 3 h. In several preliminary experiments, the effect of different ocean and atmosphere initial conditions was explored. Reducing the wind strength and deepening the ocean thermocline resulted in slower and less intense upwelling and a reduced influence of the coupling, but the qualitative response was similar to the case described here. The simulations described here were also duplicated with horizontal grid spacing reduced to 500 m, with no substantial changes to the results.

4. Modeling results

a. Uncoupled case: SST and surface currents

In the uncoupled case, the ocean model was driven by the wind stress and heat flux from the atmospheric model, but the variable SST from the ocean model was not passed back to the atmospheric model. Instead, the SST boundary condition in the atmospheric model was held fixed at its initial uniform value. Consequently, in the uncoupled case there was no mechanism to force spatial variations in the air–sea exchange processes, and wind stress and net heat fluxes remained spatially uniform in the cross-shore direction (Fig. 3).

The response in the uncoupled case was familiar from many previous studies of two-dimensional wind-driven coastal upwelling (e.g., Federiuk and Allen 1995). Offshore Ekman transport driven by the spatially uniform wind stress caused horizontal transport divergence and upwelling of cold subsurface water adjacent to the coastal boundary. Nearshore SST dropped by about 4°C during the 72-h run (Fig. 4, top). The coldest SST was found about 4 km off the coast, with slightly warmer temperatures in the shallowest water immediately adjacent to the coastal boundary. Surface currents in the end of the simulation revealed an alongshore upwelling jet developed in the near shore (Fig. 5a). The peak surface currents were almost 0.8 m s^{-1} at about 7–9 km off the coast and gradually decreased seaward to about 0.2 m s^{-1} at 40-km distance. The alongshore surface flow decreased rapidly onshore between 7 and 2 km off the coast and reversed toward stronger flow immediately adjacent to the coastal boundary.

b. Coupled case: SST and surface currents

When the model ocean and atmosphere were coupled by passing the ocean model SST to the atmo-

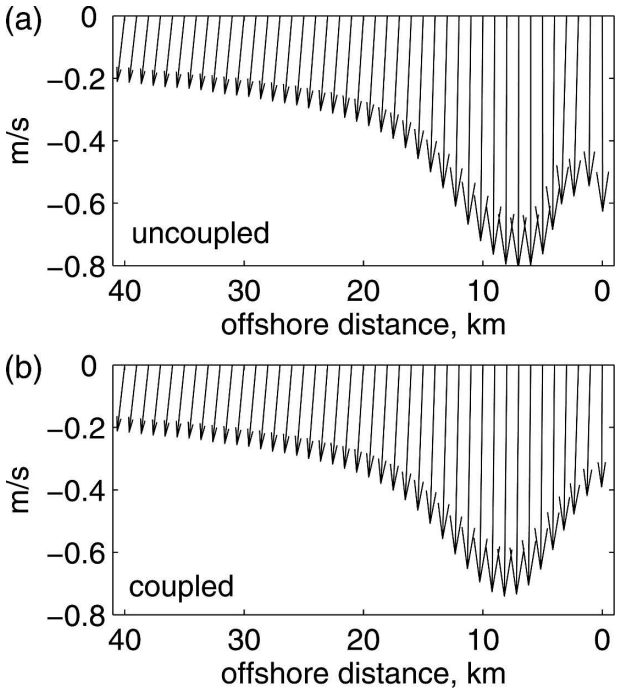

FIG. 5. Ocean surface currents in a 72-h forecast along the cross-shore line for (a) uncoupled and (b) coupled cases.

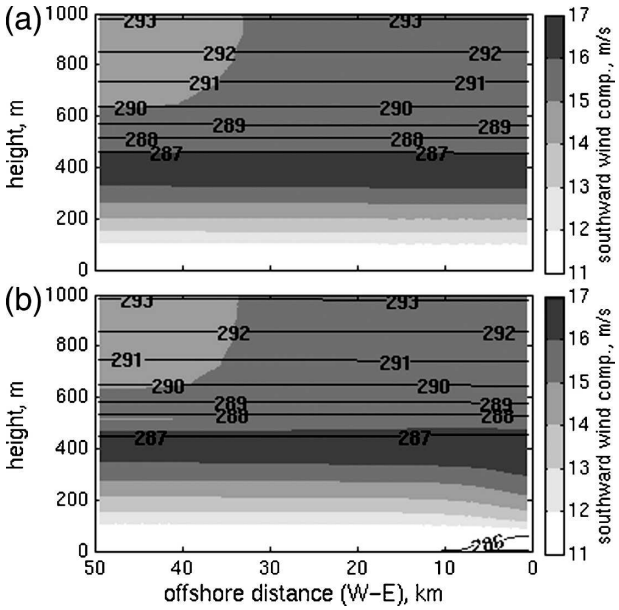

FIG. 6. Cross section of the air potential temperature (contours) and meridional wind component (shading) in the low troposphere at the final simulation time for (a) uncoupled and (b) coupled cases.

spheric model, substantial changes resulted in the air–sea fluxes in the upwelling zone. In contrast to the spatially uniform surface stress in the uncoupled case, the fully coupled case generated nearly a twofold decrease in meridional wind stress in the cross-shore direction, from 0.14 N m^{-2} offshore to 0.075 N m^{-2} near the coast (Fig. 3a). This is one of the most important results of our study. The processes responsible for this dramatic decrease in wind stress near the coastal boundary are analyzed in detail below.

Net heat flux in the coupled case increased from unstable atmospheric conditions in the offshore (upward net flux of 86 W m^{-2}; Fig. 3b) to nearly neutral or weakly stable conditions near the coast (downward net heat flux of 7 W m^{-2}) in the 72-h forecast. Note that this time corresponded to 0400 LST, so that solar radiation did not contribute to the heat flux. Offshore values of wind stress and net heat flux did not differ between the cases, as the effects of upwelling were confined within roughly 20 km off the coast through the end of the simulation.

Over the 72-h duration of these simulations, the primary differences between the coupled and uncoupled cases were found in the atmospheric boundary layer and the air–sea fluxes. However, alteration of the stress in the coupled case was sufficient to cause measurable, though not dramatic, changes in the ocean response. The SST differences between the two cases (Fig. 4, bottom) were notable within 10 km off the coast and reached 0.5°C, either positive or negative, in the inner 4 km. Surface currents in the coupled case resulted in a coastal jet maximum similar in magnitude (about 0.05 m s^{-1} weaker) and offshore location (Fig. 5b). Inshore of the jet, surface current decreased shoreward consistently in the coupled case; a similar shoreward decrease in the uncoupled case was followed by an abrupt increase adjacent to the coast.

c. Marine atmospheric boundary layer response

In the uncoupled case, the constant SST caused the potential temperature profiles to remain uniform in the cross-shore direction throughout the simulation (Figs. 6a and 7a). The profiles revealed a well-mixed marine boundary layer (MBL) and a capping inversion with base at about 450 m that were formed by the end of the simulation across the entire domain. Turbulent properties in the well-mixed boundary layer were also horizontally uniform in the uncoupled case (Fig. 8).

In contrast, the potential temperature vertical profiles and cross section at the end of the coupled simulation show a well-mixed MBL in the offshore region but a developing internal boundary layer (IBL) over the colder upwelled water within 10 km off the coast (Figs. 6b and 7a). The upper part of the offshore MBL was about 0.3°–0.4°C warmer and slightly more elevated in the coupled case, as a result of the warmer

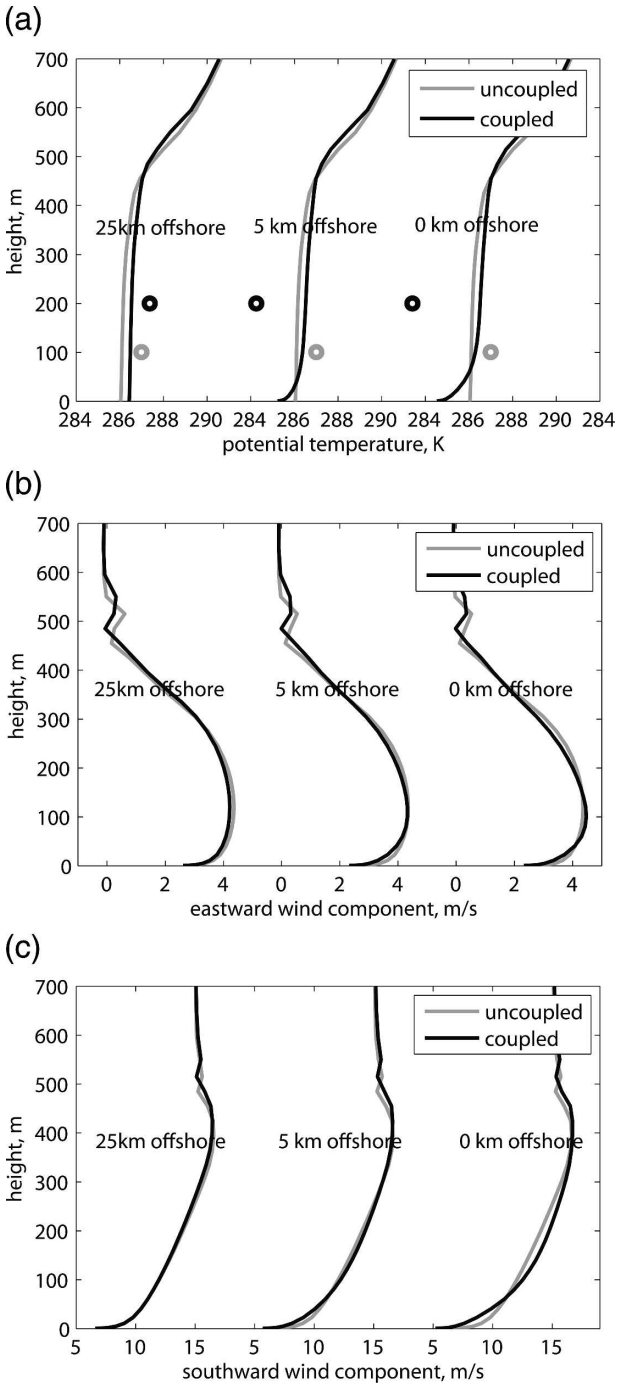

FIG. 7. Vertical profiles at three offshore locations for a 72-h simulation: (a) atmospheric potential temperature and the underlying SST marked by black (gray) circles for the coupled (uncoupled) simulation, (b) zonal (eastward) wind, and (c) meridional (southward) wind. Note that the SST in the uncoupled case is held constant in the atmospheric model, and so it differs from the SST of the ocean model shown in Fig. 4 for the corresponding simulation.

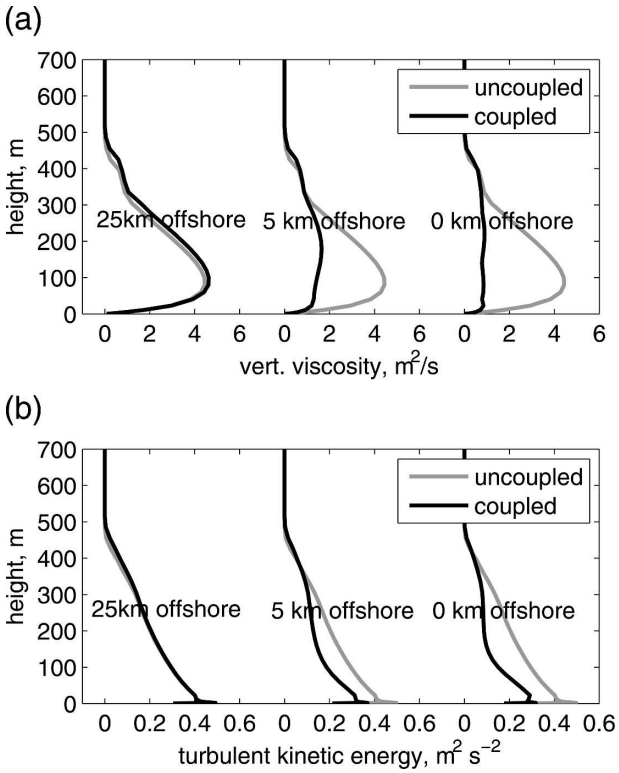

FIG. 8. Atmospheric vertical profiles at three offshore locations, after a 72-h simulation: (a) vertical mixing coefficient and (b) turbulent kinetic energy.

SST. At inshore locations, SST in the coupled case was consistently cooler than the surface air temperature, suggesting that onshore advection maintained a slightly warmer boundary layer relative to the upwelled water.

In both cases, an area of supergeostrophic southward wind component was evident just below the capping inversion across the domain. In the coupled case, an additional intensification of this feature occurred above the IBL within 10 km of the coast (Fig. 6b, shaded contours). Initially, in both cases, the boundary layer flow was in a three-way balance between pressure gradient force, Coriolis force, and vertical turbulent stress divergence. This balance produced slight onshore flow in the atmospheric boundary layer crossing the pressure gradient (Fig. 7b). In both the coupled and uncoupled cases, reduction in the stress divergence term above the boundary layer caused a flow imbalance and acceleration of the alongshore flow. Since there was no alongshore pressure gradient, the alongshore momentum balance remained that of a weakly stratified Ekman layer, with the Coriolis force from the modified onshore flow balancing the stress divergence. The cross-shore balance remained geostrophic to first order, with the Ekman stress modification near the surface. In the

coupled case, the IBL that developed adjacent to the coast modified the vertical stress divergence, leading to weaker alongshore flow near the surface and stronger alongshore flow in the boundary layer above 100 m (Figs. 6b and 7c). The cross-shore wind was also slightly weaker near the surface in the coupled case, with stronger wind shear above the IBL (Fig. 7b).

Profiles of mixing properties from the lower troposphere (Fig. 8) are consistent with this interpretation. For example, in the nearshore region, the coupled case produced vertical viscosity values that were a factor of 4 smaller than the uncoupled case. Turbulent kinetic energy (TKE) was also smaller in the coupled case throughout the lower 400 m of the MBL. At a location 25 km offshore, differences were not as significant and were likely related to the elevated boundary layer height produced in the coupled case. Note also that in the offshore region TKE decreased nearly linearly from its maximum near the surface to the top of the MBL. In contrast, at 5 km offshore and at coastal points, TKE profiles showed a more rapid decrease in the lower 100–200 m in the coupled case, with much lower values above that height up to a height of ~400 m. The two-layer structure presented over the colder upwelled water was similar to boundary layer observations of flow from warm to cold water (Skyllingstad et al. 2005). Small TKE values between 100 and 400 m represented an uncoupled boundary layer advected by weak zonal winds from offshore, or weak locally generated turbulence in the weakly stratified remnant boundary layer above the IBL.

d. Ekman transport and the ocean surface layer

Wind-forced upwelling can result from both coastal divergence of Ekman transport in the ocean boundary layer and from offshore Ekman layer divergence due to the wind stress curl away from the coast (Ekman pumping). In our simulations, we considered only two-dimensional fields with uniform alongshore flow, thereby limiting wind stress curl calculations to the meridional wind stress component (Fig. 9a). The coupled case yielded positive wind stress curl in the nearshore 20 km; peak curl values occur about 7 km off the coast. Cross-shore wind stress in the uncoupled case was constant and, therefore, resulted in zero curl.

The local cross-shore Ekman transport M_E (Fig. 9b) was computed as $M_E = -\tau_y/\rho f$, where ρ is water density (assumed constant here), f is the Coriolis parameter, and τ_y is the meridional component of surface wind stress. Reduction of the nearshore wind stress caused a ~50% decrease in Ekman transport near the coast relative to the uncoupled case. Ekman transport in the coupled case increased with offshore distance and reached values similar to the uncoupled case at 15–20 km off the coast.

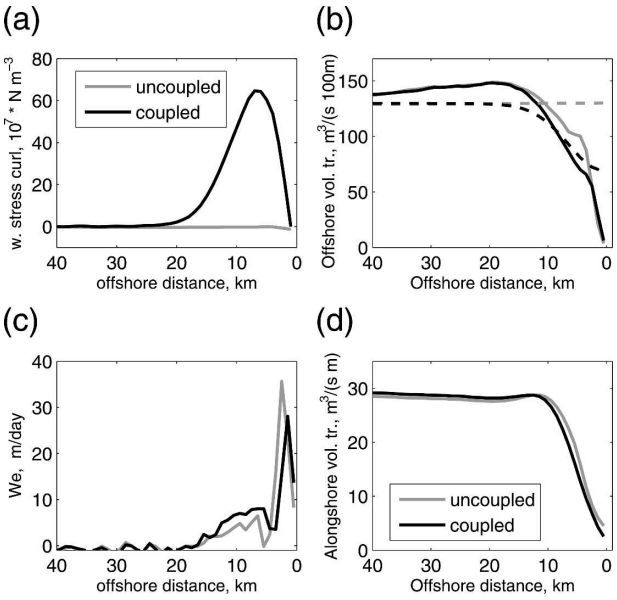

FIG. 9. (a) Model wind stress curl computed from meridional wind stress shown in Fig. 3a; (b) vertically integrated offshore volume transport in the ocean surface layer from model results (solid lines) and offshore transport estimated from wind stress forcing (dashed lines); (c) vertical velocity at the base of the surface layer (also see text); (d) total depth-integrated alongshore volume transport.

The offshore transport in the surface layer was also computed directly by integrating downward from the surface over a surface layer defined by the contiguous extent of offshore flow (Fig. 9b). Depth-integrated offshore transports were similar for the two cases at distances greater than 15 km. Between 3 and 15 km, the depth-integrated offshore transport was systematically larger in the uncoupled case, by as much as 30%. Immediately adjacent to the coast, this transport was smaller for the uncoupled case. Development of classical upwelling circulation in the shallow near-coastal region appeared to be affected by interaction of the surface and bottom boundary layers. Note that the difference of the Ekman and depth-integrated offshore transport estimates was about 10%–15% in the offshore region.

Upwelling velocities at the base of the offshore flow surface layer, defined above, were estimated as vertical velocities at the depth with zero zonal flow (Fig. 9c). These upwelling velocities indicate the intensity of entrainment into the surface layer from the ocean interior. At the coast, weaker values for the uncoupled case were notable in comparison with the coupled case, with corresponding magnitudes of 8.3 and 13.6 m day^{-1}. The

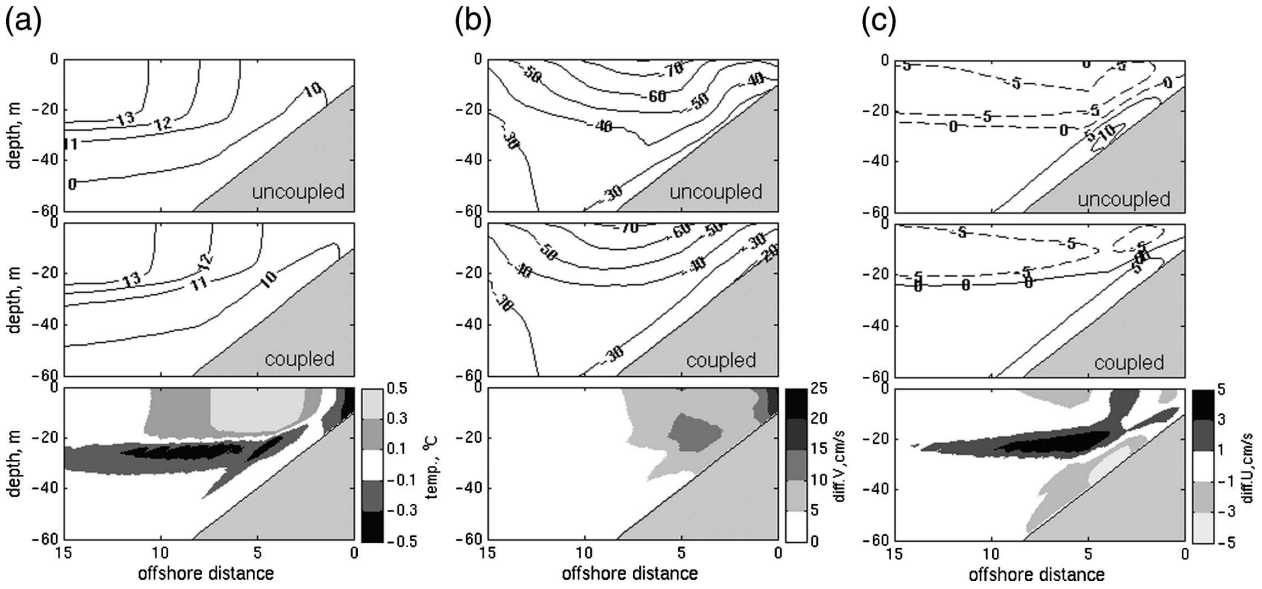

FIG. 10. Ocean cross sections in the nearshore 20-km region at the end of a 72-h simulation: (a) temperature, (b) v velocity, and (c) u velocity. (top) Uncoupled and (middle) coupled simulation; (bottom) the differences between the corresponding fields in the coupled and uncoupled cases.

largest magnitudes of the entrainment were within 2–3 km offshore; peak value for the uncoupled case was 35.6 m day^{-1} at the third grid point from the coast and 28.1 m day^{-1} for the coupled case at the second grid point from the coast. Upwelling velocities decreased rapidly moving offshore, with consistently higher values for the coupled case.

Alongshore volume transport, computed as the vertical integral of the meridional flow over the full fluid depth, was consistently higher for the uncoupled case in the nearshore 15 km (Fig. 9d). The lack of coastal wind reduction in the uncoupled case thus resulted in an overestimate of the alongshore volume transport in comparison with the coupled simulation.

e. Coastal ocean response

Differences in the ocean circulation are apparent in vertical cross sections of model variables from the coupled and uncoupled cases (Fig. 10). In both cases, the surface layer remained well mixed in temperature from the surface down to about 20-m depth at 15 km or more distance from the coast and is not shown. At distances of 5–15 km, the surface layer appeared to be mixed to a slightly greater depth in the uncoupled case. This resulted in colder temperatures across the surface mixed layer in the uncoupled case, consistent with colder SST shown above (Fig. 4) for the corresponding offshore distances. A warmer surface layer to 20-m depth at distances between about 3 and 10 km off the coast in the coupled case was above the cooler layer located approximately between 20 and 35 m (Fig. 10a, bottom). This colder layer extended inshore and up to the ocean surface at the inshore 1–2 km distance (cf. to Fig. 4).

Cross section of the meridional flow showed no difference between the cases at distances greater than 15 km from the coast; by that reason only the area inshore 15 km is presented in Fig. 10b. In that region, a southward jet was forced over the coastal slope in both cases, centered at 7–9 km off the coast, corresponding to the surface flow maxima in Fig. 5. The jet had a more asymmetric and irregular structure in the uncoupled case in comparison with the coupled. In the uncoupled case, the peak velocities were located over a deeper surface mixed layer, diverting the 40 cm s^{-1} isopleth to a greater depth 7 km offshore. In addition, greater wind stress inshore of the jet peak caused greater downward mixing of momentum, which resulted in stronger currents near the coast than in the coupled case. In the coupled case, the southward jet exhibited a smoother and more symmetrically shaped structure across the water depth, and the flow speed changed consistently in the shallow region inshore of 5 km. Greatest differences between the cases of 10–15 cm s^{-1} resulted at the last two inshore grid points, and differences of about 10 cm s^{-1} resulted at about a 4–5-km distance from the coast at the ocean surface and at approximately 20-m depth.

Zonal velocity cross sections (Fig. 10c) display well-

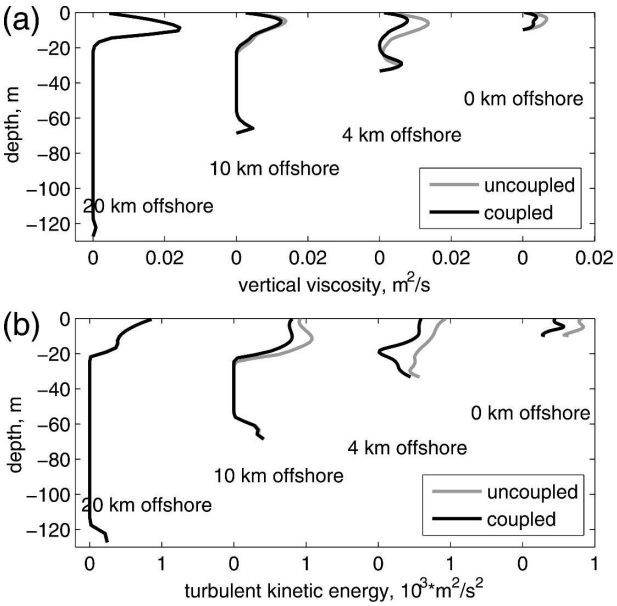

FIG. 11. (a) Oceanic vertical profiles of viscosity coefficients for a 72-h forecast, 0400 LST, and (b) turbulent kinetic energy for the same time.

defined offshore flow in the upper ~20 m, outlining the surface layer characterized by offshore transport. Maximum offshore zonal velocities were found near the surface across the water column about 15 km or more offshore. The offshore flow maxima became subsurface at 4–15 km distances from the coast. Subsurface maximum of the onshore zonal flow reached greater magnitudes in the uncoupled case (Fig. 10c, bottom). Note also that at approximately 5 km from the coast, offshore flow (negative values) in the uncoupled case extended to a slightly greater depth. These differences could be attributed to stronger surface wind stress in the uncoupled case in the nearshore region that lead to surface layer deepening between 4 and 15 km. Shallow depths at distances closer than 4 km to the coastline limited surface boundary layer development. Surface wind stress was also balanced by the bottom stress in this region. More discussion on offshore transport in the surface layer has been presented in section 4d.

Variations in vertical thermal and horizontal flow structure discussed above suggest that turbulent mixing of momentum may have played a key role in causing the differences between the uncoupled and coupled cases in the nearshore region. Importance of mixing may be estimated from vertical profiles of turbulent properties at several offshore locations (Fig. 11). At 20 km offshore, the two cases showed almost no difference for either of the variables. At 10 km offshore, vertical viscosity was slightly smaller in the coupled case; peak value of TKE was ~20% larger in the uncoupled case. The model did not resolve subscale turbulent motions, and therefore TKE was expected to reduce to zero in the ocean interior. Accordingly, TKE profiles 20 and 10 km offshore in both cases exhibited a clear distinction between the surface and bottom boundary layers that were characterized by regions of increased mixing near the top and bottom, separated by nonturbulent mid-depth region. At 4 km, viscosity profiles indicated weaker mixing in the surface layer for the coupled case, with peak values nearly one-half of the uncoupled case. Corresponding TKE profiles for the location not only agreed on the reduced mixing result for the coupled case but demonstrated the qualitative difference between the two cases. TKE values remained elevated across the water column in the uncoupled case, while reaching a minimum with near-zero values in the middle of the profile in the coupled case. This is an indication of surface and bottom boundary layers overlapping in the uncoupled case and remaining separate in the coupled case. At the coast (rightmost profiles), reduced mixing was predicted for the coupled case in both variables. TKE remained elevated across the water column for both cases but was about 2 times as high in the uncoupled case than in the coupled case.

Qualitative estimates of the surface boundary layer (SBL) depth from Figs. 10 and 11 suggest that the SBL became more shallow between 5 and 15 km offshore in the coupled case but remained at the same depth or deepened slightly in the uncoupled case (Fig. 10c). Inshore of 5 km at ~40 m or less water depth, the SBL and bottom boundary layer overlapped, physically restricting surface boundary layer development.

5. Discussion

The coupled simulation reported here demonstrates that SST variations from wind-driven coastal upwelling can cause major changes in the marine atmospheric boundary layer structure and wind stress in the coastal zone on time scales of 72 h or less. Formation of the internal boundary layer in the atmosphere, with the accompanying reduction by one-half of the local wind stress, over the cold upwelled water on the inner shelf was unique to the coupled ocean–atmosphere case. No such feature formed in the uncoupled case. The results demonstrate that the changes in coastal zone wind stress resulting from this interaction can be comparable in magnitude to the stress that initiates the upwelling circulation. These changes in stress are substantially larger than those obtained from consideration of stability effects on bulk aerodynamic fluxes alone (e.g., Enriquez and Friehe 1995), because the entire structure of the boundary layer is affected, changing the near-

surface winds along with the local stability. The air–sea interaction creates a decoupled boundary layer system, where air–sea momentum and heat fluxes only affect the shallow internal boundary layer, creating an effective bottom boundary for the remaining atmosphere that is much like a free-slip condition with minimal heat and moisture fluxes. The results show also that high vertical resolution in the marine boundary layer near the ocean surface will be required for accurate modeling of these processes, as the local internal boundary layer thickness may be only a few tens of meters or less.

The coupled simulation is generally consistent with recent in situ and aircraft observations of the coastal marine atmospheric boundary layer off Oregon, which have indicated that wind-driven coastal upwelling circulation can reduce sea surface temperatures near the coast 4°C or more when compared with corresponding SST farther offshore (Samelson et al. 2002; Bane et al. 2005). The simulated development of the IBL agrees qualitatively with the Bane et al. (2005) observations of the lower troposphere and ocean off the Oregon coast during the Coastal Observation and Simulation with Topography (COAST) experiment on 24–25 July 2001. Both modeled and observed results indicate a well-mixed MBL with a capping inversion at 450–500 m, a region of higher southward flow below the inversion base, and a stable IBL above the cool upwelled water near the coast. Observational and numerical studies of offshore flow of warm air over cold water in other locations have shown similar results, including the development of a shallow IBL and rapid turbulence decay above in the remnant MBL (Vickers et al. 2001; Skyllingstad et al. 2005).

Despite highly idealized conditions in our simulations, the simulated ocean state is qualitatively similar to observed conditions along the U.S. West Coast, such as those described in the observational study by Huyer et al. (2005), which was based on the 5-year hydrographic surveys made during the Global Ocean Ecosystems Dynamics (GLOBEC) program. Figure 6b of Huyer et al. (2005) shows the SST along 44.6°N (off Newport, Oregon) with the coldest water of ~10.5°C near the coast, a sharp cross-shore temperature gradient in the next 40 km, and temperatures reaching about 15.5°C 50 km off the coast. Mixed layer depth in their Fig. 6d is about 10 m or less along the same transect, unlike the highly variable and generally thicker mixed layer depth farther south off Cape Blanco, Oregon (42.9°N), where coastal flow–topography interaction complicates the circulation. Mean geostrophic surface currents in their Fig. 7b off Newport indicate a peak surface jet of ~50 cm s^{-1} found 15 km off the coast that rapidly decelerates to 0.25 cm s^{-1} inshore, with slower deceleration to less than 10 cm s^{-1} at 100-km offshore distance. The same study also reported that the band of cool water (<13°C) at the surface was ~20 km wide off Newport. Note that the resulting temperatures at the coast (about 10.5°–11°C) and offshore (about 15.5°C 50 km off the coast) in our numerical simulations are very similar to the observed values, as is the qualitative cross-shore pattern of surface currents. This overall quantitative similarity gives added confidence that the conclusions from the coupled simulation are relevant to the coastal ocean.

The modeled coastal ocean response in the coupled case supports several findings by Lentz (1992), Dever (1997), and Dever et al. (2006). First, the near-surface offshore transport is similar in magnitude to the Ekman transport derived from wind stress in the offshore and most of the coastal region. This contrasts with the uncoupled simulation, in which the offshore transport is much weaker than the Ekman transport in the region of Ekman divergence. Both simulations showed weaker offshore transport inshore of 4 km, approximately corresponding to an inner shelf regime in which internal turbulent stresses and bottom drag combine to reduce the offshore transport. Second, the reduction of surface wind over the cool water in the coupled simulation caused the adjustment of Ekman divergence to occur gradually with offshore distance, and the corresponding ocean surface boundary layer is relatively shallow near the coast and grows deeper with offshore distance. In the absence of the wind reduction, such adjustment would occur over a very short offshore distance, and the surface boundary layer would remain of similar depth beyond that distance (Fig. 3 in Lentz 1995) with weak entrainment from the ocean interior. Our results show relatively strong vertical velocities near the coast, and offshore transport increasing more rapidly offshore, in the uncoupled case (Fig. 9).

Several recent observational and modeling studies have suggested that wind stress may be systematically reduced within 100 km of the Oregon coast, relative to values farther offshore (Samelson et al. 2002; Perlin et al. 2004; Bane et al. 2005), but the uncertainties in these estimates remain large. Satellite scatterometer measurements (Perlin et al. 2004) are not available within roughly 25 km of the coast and so are insufficient for model validation in that region, which is roughly the offshore extent of SST-induced wind reduction in the coupled simulation. Note that the location of this coastal wind reduction strongly depends on the offshore penetration of cold waters near the coast, and therefore, on the stage of upwelling development. On larger scales, satellite observations do show correlations of SST and stress (Chelton et al. 2007). Upwelling

velocity in the coupled model varied substantially over the nearshore 20-km distance. Peak model values were roughly one order of magnitude greater than scatterometer estimates of the upwelling velocity for summertime conditions off the Oregon coast (about 28.1 m day^{-1} in the coupled case versus about 2 m day^{-1} in Fig. 13 in Huyer et al. 2005). The scatterometer estimates were obtained by dividing the offshore volume transport by the 10–20-km width of the coastal region where the cross-shelf divergence was assumed to occur. Comparable model estimates, averaged over a 15-km coastal region, resulted in values for the uncoupled and coupled cases of 7.8 and 8.2 m day^{-1}, respectively. The difference between coupled and uncoupled cases is small but suggests slightly greater entrainment at the base of the Ekman layer for the coupled simulation.

In the coupled simulation, the air–sea heat fluxes near the beginning of the simulation (hours 3–12) were about -5 to -7 W m^{-2} for sensible heat (SHF) and 30–35 W m^{-2} for latent heat (LHF), similar to the monthly fields of heat fluxes from the sequential atmospheric model 12-h forecasts reported by Haack et al. (2005) who found SHF of -10 W m^{-2} for stable conditions and LHF as small as 20 W m^{-2} in July north of Point St. George and Point Reyes off the northern California coast. After the model adjustment and by the end of the 72-h run, the numbers for the inshore and offshore locations differed both from these values and from each other: at 20 km offshore, SHF was -3 W m^{-2} and LHF was 1–2 W m^{-2}, while at a coastal point, SHF was -30 W m^{-2} and LHF was -42 W m^{-2}. At the coastal point, the difference between the sum of the initial and final SHF and LHF was about 100 W m^{-2}. The amplitude of these changes suggests that coupled models with evolving SST fields may yield substantially different heat flux fields on the mesoscale forecast time scale.

6. Summary and conclusions

The present study was designed to investigate the effects of ocean–atmosphere coupling in a simple two-dimensional coastal wind-driven upwelling scenario motivated by observed conditions along the central Oregon coast. Within 20 km off the coast, wind stress was reduced to half of its offshore value in the 72-h coupled ocean–atmosphere simulation. This change in stress due to air–sea coupling is substantially larger than that predicted by some previous studies, such as by Enriquez and Friehe (1995). The major reason for this difference is that, in the coupled model, the atmospheric boundary layer structure is fundamentally altered by air–sea fluxes over the cold upwelled water through the development of a stable internal boundary layer. The increased stability of the entire boundary and weaker turbulence in the internal boundary layer in the coupled simulation were consistent with previous observational studies. In contrast, previous studies predicting weaker coupling have focused on the stability dependence of drag coefficients, with a fixed near-surface wind.

Even during the relatively brief 72-h duration of these simulations, some effects of the coupling were apparent in the ocean response. Between 3 and 15 km from the coast, offshore transport in the ocean surface boundary layer increased more rapidly with offshore distance, and vertical velocities at the base of the surface layer were stronger, for the coupled case. The coupled case also generated a thinner nearshore surface layer with gradual seaward deepening. Overall, adjustment of surface Ekman divergence to the coastal boundary occurred over greater offshore distance in the coupled case than in the uncoupled case. Weaker nearshore wind stresses in the coupled case also resulted in consistently smaller alongshore transport in the oceanic surface layer. Because of the reduced stress in the coupled case, vertical mixing in the upwelling zone was weaker, resulting in a shallower surface mixed layer. This delayed the merging of the surface and bottom boundary layers over the inner shelf and allowed further inshore propagation of the bottom upwelling front. Within 2 km off the coast, local cross-shore transport estimates were slightly greater and SST slightly cooler for the coupled case. It should be emphasized that the inner shelf region, loosely defined as the region in which surface and bottom boundary layer interact, remains poorly understood and difficult to observe and model, and the model results depend in part on imperfect parameterizations of boundary layer turbulence, so that conclusions about these dynamics based purely on simulations must be treated with caution.

The coupled model in the idealized configuration was able to reproduce conditions typical for the summertime coastal circulation off the Oregon coast. Results of the coupled simulations were generally consistent, in a qualitative sense, with ocean and atmosphere observations made during the upwelling season off central Oregon. The results described here indicate that air–sea interaction on short temporal and horizontal scales may play a central role in controlling essential elements of inner-shelf circulation. They should be seen as a modest step toward a more comprehensive understanding of ocean–atmosphere interaction in the coastal zone and its effect on the coastal ocean response to synoptic atmospheric conditions. Planned extensions of this research include the coupled simulation of three-di-

mensional flows with coastal land topography and bathymetry similar to the coastal regions along Oregon and California. Other possible future extensions include the addition of freshwater sources, such as the Columbia River plume as well as simulations focusing more generally on the effects of variable stratification in the coastal ocean, and investigation of the role of air–sea interaction in low-level coastal stratus formation in the atmosphere.

Acknowledgments. This research was supported by Grants N00014-01-1-0231 and N00014-06-1-0328 from the Office of Naval Research and Award NA03-NES4400001 to Oregon State University from the National Oceanic and Atmospheric Administration (NOAA), U.S. Department of Commerce. The statements, findings, conclusions, and recommendations are those of the authors and do not necessarily reflect the views of NOAA or the Department of Commerce.

REFERENCES

Allen, J. S., P. A. Newberger, and J. Federiuk, 1995: Upwelling circulations on the Oregon continental shelf. Part I: Response to idealized forcing. *J. Phys. Oceanogr.,* **25,** 1843–1866.

Bane, J. M., M. D. Levine, R. M. Samelson, S. M. Haines, M. F. Meaux, N. Perlin, P. M. Kosro, and T. Boyd, 2005: Atmospheric forcing of the Oregon coastal ocean during the 2001 upwelling season. *J. Geophys. Res.,* **110,** C10S02, doi:10.1029/2004JC002653.

Burk, S. D., T. Haack, and R. M. Samelson, 1999: Mesoscale simulation of supercritical, subcritical, and transcritical flow along coastal topography. *J. Atmos. Sci.,* **56,** 2780–2795.

Chelton, D. B., and Coauthors, 2001: Observations of coupling between surface wind stress and sea surface temperature in the eastern tropical Pacific. *J. Climate,* **14,** 1479–1498.

——, M. G. Schlax, and R. M. Samelson, 2007: Summertime coupling between sea surface temperature and wind stress in the California Current System. *J. Phys. Oceanogr.,* **37,** 495–517.

Dever, E. P., 1997: Wind-forced cross-shelf circulation on the northern California shelf. *J. Phys. Oceanogr.,* **27,** 1566–1580.

——, C. E. Dorman, and J. L. Largier, 2006: Surface boundary layer variability off northern California, USA, during upwelling. *Deep-Sea Res. II,* **53,** 2887–2905.

Enriquez, A. G., and C. A. Friehe, 1995: Effects of wind stress and wind stress curl variability on coastal upwelling. *J. Phys. Oceanogr.,* **25,** 1651–1671.

Federiuk, J., and J. S. Allen, 1995: Upwelling circulation on the Oregon continental shelf. Part II: Simulations and comparisons with observations. *J. Phys. Oceanogr.,* **25,** 1867–1889.

Gan, J., J. S. Allen, and R. M. Samelson, 2005: On open boundary conditions for a limited-area coastal model off Oregon. Part 2: Response to wind forcing from a regional mesoscale atmospheric model. *Ocean Modell.,* **8,** 155–173.

Haack, T., S. D. Burk, and R. M. Hodur, 2005: U.S. west coast surface heat fluxes, wind stress, and wind stress curl from a mesoscale model. *Mon. Wea. Rev.,* **133,** 3202–3216.

Halpern, D., 1976: Structure of a coastal upwelling event observed off Oregon during July 1973. *Deep-Sea Res.,* **23,** 495–508.

Harshvardhan, R. Davies, D. A. Randall, and T. G. Corsetti, 1987: A fast radiation parameterization for atmospheric circulation models. *J. Geophys. Res.,* **92,** 1009–1016.

Hodur, R. M., 1997: The Naval Research Laboratory's Coupled Ocean/Atmosphere Mesoscale Prediction System (COAMPS). *Mon. Wea. Rev.,* **125,** 1414–1430.

Huyer, A., 1983: Coastal upwelling in the California Current system. *Prog. Oceanogr.,* **12,** 259–284.

——, J. H. Fleischbein, J. Keister, P. M. Kosro, N. Perlin, R. L. Smith, and P. A. Wheeler, 2005: Two coastal upwelling domains in the northern California Current system. *J. Mar. Res.,* **63,** 901–929.

Large, W. G., J. C. McWilliams, and S. C. Doney, 1994: Oceanic vertical mixing: A review and a model with a nonlocal boundary layer parameterization. *Rev. Geophys.,* **32,** 363–403.

Larson, J., R. Jacob, and E. Ong, 2005: The Model Coupling Toolkit: A new Fortran90 toolkit for building multiphysics parallel coupled models. *Int. J. High Perf. Comput. Appl.,* **19,** 277–292.

Lentz, S. J., 1992: The surface boundary layer in coastal upwelling regions. *J. Phys. Oceanogr.,* **22,** 1517–1539.

——, 1995: U.S. contributions to the physical oceanography of continental shelves in the early 1990's. *Rev. Geophys.,* **33** (Suppl.)*,* 1225–1236.

Louis, J. F., 1979: A parametric model of vertical eddy fluxes in the atmosphere. *Bound.-Layer Meteor.,* **17,** 187–202.

Marchesiello, P., J. C. McWilliams, and A. Shchepetkin, 2001: Open boundary conditions for long-term integration of regional ocean models. *Ocean Modell.,* **3,** 1–20.

Mellor, G. L., and T. Yamada, 1982: Development of a turbulence closure model for geophysical fluid problems. *Rev. Geophys. Space Phys.,* **20,** 851–875.

Miller, M. J., and A. J. Thorpe, 1981: Radiation conditions for the lateral boundaries of limited-area numerical models. *Quart. J. Roy. Meteor. Soc.,* **107** (C5), 21–29.

Perlin, N., R. M. Samelson, and D. B. Chelton, 2004: Scatterometer and model wind and wind stress in the Oregon–northern California coastal zone. *Mon. Wea. Rev.,* **132,** 2110–2129.

Pickett, M. H., and J. D. Paduan, 2003: Ekman transport and pumping in the California Current based on the U.S. Navy's high-resolution atmospheric model (COAMPS). *J. Geophys. Res.,* **108,** 3327, doi:10.1029/2003JC001902.

Samelson, R. M., and Coauthors, 2002: Wind stress forcing of the Oregon coastal ocean during the 1999 upwelling season. *J. Geophys. Res.,* **107,** 3034, doi:10.1029/2001JC000900.

Shchepetkin, A. F., and J. C. McWilliams, 2005: The Regional Ocean Modeling System (ROMS): A split-explicit, free-surface, topography-following coordinate oceanic model. *Ocean Modell.,* **9,** 347–404.

Skyllingstad, E. D., R. M. Samelson, L. Mahrt, and P. Barbour, 2005: A numerical modeling study of warm offshore flow over cool water. *Mon. Wea. Rev.,* **133,** 345–361.

Smith, R. L., 1974: A description of current, wind, and sea level variations during coastal upwelling off the Oregon coast, July–August 1972. *J. Geophys. Res.,* **79,** 435–443.

Vickers, D., L. Mahrt, J. Sun, and T. Crawford, 2001: Structure of offshore flow. *Mon. Wea. Rev.,* **129,** 1251–1258.